Reduction of neurovascular damage resulting from microelectrode insertion into the cerebral cortex using *in vivo* two-photon mapping

2010 J. Neural Eng. 7 046011

(http://iopscience.iop.org/1741-2552/7/4/046011)

J. Neural Eng. **7** (2010) 046011 (12pp) doi:10.1088/1741-2560/7/4/046011

Reduction of neurovascular damage resulting from microelectrode insertion into the cerebral cortex using *in vivo* two-photon mapping

T D Y Kozai[1], T C Marzullo[1], F Hooi[2], N B Langhals[1], A K Majewska[3], E B Brown[4] and D R Kipke[1]

[1] Neural Engineering Lab, Department of Biomedical Engineering, College of Engineering, University of Michigan, Ann Arbor, MI, 48109, USA
[2] Basic Radiological Sciences Division, Department of Biomedical Engineering, College of Engineering, University of Michigan, Ann Arbor, MI, 48109, USA
[3] Department of Neurobiology and Anatomy, School of Medicine and Dentistry, University of Rochester, Rochester, NY, 14642, USA
[4] Biomedical Engineering, School of Medicine and Dentistry, University of Rochester, Rochester, NY, 14642, USA

E-mail: tkozai@umich.edu and dkipke@umich.edu

Received 1 February 2010
Accepted for publication 22 June 2010
Published 19 July 2010
Online at stacks.iop.org/JNE/7/046011

Abstract
Penetrating neural probe technologies allow investigators to record electrical signals in the brain. The implantation of probes causes acute tissue damage, partially due to vasculature disruption during probe implantation. This trauma can cause abnormal electrophysiological responses and temporary increases in neurotransmitter levels, and perpetuate chronic immune responses. A significant challenge for investigators is to examine neurovascular features below the surface of the brain *in vivo*. The objective of this study was to investigate localized bleeding resulting from inserting microscale neural probes into the cortex using two-photon microscopy (TPM) and to explore an approach to minimize blood vessel disruption through insertion methods and probe design. 3D TPM images of cortical neurovasculature were obtained from mice and used to select preferred insertion positions for probe insertion to reduce neurovasculature damage. There was an 82.8 $\pm$ 14.3% reduction in neurovascular damage for probes inserted in regions devoid of major (>5 μm) sub-surface vessels. Also, the deviation of surface vessels from the vector normal to the surface as a function of depth and vessel diameter was measured and characterized. 68% of the major vessels were found to deviate less than 49 μm from their surface origin up to a depth of 500 μm. Inserting probes more than 49 μm from major surface vessels can reduce the chances of severing major sub-surface neurovasculature without using TPM.

(Some figures in this article are in colour only in the electronic version)

1. Introduction

High fidelity, permanent, implantable microscale neural interface devices are enabling components for a broad class of scientific and emerging clinical applications. The capability of monitoring specific neuronal ensembles using these probes for long periods of time with great precision would be a powerful tool in neuroscience research for linking low-level neuronal circuits to high-level brain function, such as learning, memory and perception. In clinical areas, it would

enable the development of closed-loop neurostimulation and neuroprosthetic systems using multichannel unit activity or local field potentials. A growing body of work provides evidence that long-term neuro-implants for spike recording are feasible (Kipke *et al* 2008, Schmidt *et al* 1976). This work can be summarized through four overall findings: (1) one can typically record useful spike activity from the cortex and deeper structures for more than 6 months using any of the several types of implantable microelectrode probes; (2) the recording quality is typically adequate, but not outstanding, over this time period; (3) the quality of recordings eventually degrades to the point where they are of limited or no use, and (4) the unresolved engineering issue is to increase the quality, stability and longevity of recordings using implantable microelectrode probes. While progress is being made to improve implantable probes and to better understand the associated reactive tissue responses, the complex relationships between the structure and function in chronic neural interfaces are not well understood.

The present study is focused on the initial localized disruption of the blood brain barrier (BBB) and bleeding resulting from inserting a microscale neural probe into the cerebral cortex. This is important because acute tissue damage leads to the release of erythrocytes, clotting factors and inflammatory factors from disrupted blood vessels which facilitate the recruitment of activated microglia and a broad region of astrocyte activation around the inserted probe (Schwartz *et al* 2006, Szarowski *et al* 2003, Turner *et al* 1999, Grill *et al* 2009). During insertion, the highly regulated BBB is compromised leading to plasma protein release into the surrounding parenchyma, resulting in adsorption onto the electrode, increased concentrations of extracellular serum proteins, ions and other solutes, and deposition of plasma into the neuropil (Groothuis *et al* 1998, Kimelberg 1995). Acutely, this damage can be observed as irregularities in neuronal spike activity (Johnson *et al* 2006), elevated levels of extracellular neurotransmitters (Camp and Robinson 1992, Goldsmith *et al* 1995, Holson *et al* 1998) and a net increase in extracellular water content (Betz *et al* 1989, Klatzo 1967, Unterberg *et al* 2004). This vasogenic edema leads to increased brain tissue volume and intracranial pressure (Barzo *et al* 1997) often associated with their impact on tissue damage (Dixon *et al* 1991, McIntosh *et al* 1996) and clinical outcome (Narayan *et al* 2002). For example, albumin, the most abundant protein in blood plasma (Shen *et al* 2004), is responsible, in part, for inducing glial cell activation and proliferation (Nadal *et al* 1995, 1998,). Although stab wound studies show limited chronic tissue damage (McConnell *et al* 2009, Biran *et al* 2005), plasma protein adsorption onto the electrode may perpetuate the tissue response in chronically implanted electrodes. Furthermore, disrupting major arterioles during probe insertion can cause additional neuronal damage, by means of ischemia, through loss of perfusion to the tissue below the disrupted region, which is typically where the recording sites are located (Nishimura *et al* 2007, Zhang *et al* 2005).

Investigation of initial localized bleeding resulting from neural probe insertion is also important because there is experimental evidence that it can be affected through the electrode design and surgical technique. For example, electrode shape and insertion speed have been related to tissue damage (Johnson *et al* 2007, Bjornsson *et al* 2006, Edell *et al* 1992). The details of probe insertion may also impact chemical trauma in tissue (Johnson *et al* 2007), as the implantation of probes punctures and tears neural vasculature (House *et al* 2006, Bjornsson *et al* 2006). These types of high-resolution investigations of neurovasculature currently use postmortem histology or *ex vivo* brain tissue slice preparations. In both cases, the brain tissue under study must be excised from the native environment and extensively processed, which limits the degree to which temporal effects (both immediate and chronic) of probe insertion can be investigated.

In vivo two-photon microscopy (TPM) provides an innovative approach to studying the localized, microscale tissue effects of neural probe insertion and implantation. TPM is experiencing significant growth in biomedical research (Zipfel *et al* 2003, Svoboda and Yasuda 2006, Dunn and Sutton 2008, Lowery *et al* 2009, Majewska *et al* 2000a, Chauhan *et al* 2009) because it allows detailed observation of deeper tissue structures beyond the range of confocal microscopy (Helmchen and Denk 2005). Specifically, TPM has been used to create 2D and 3D models of vasculature associated with tumor growth (Abdul-Karim *et al* 2003, Tyrrell *et al* 2005). Our interest is to use *in vivo* TPM to generate 3D maps of the vasculature in small regions of the cortex in a live mouse in order to investigate tissue damage associated with inserting neural probes.

The objective of this study was to investigate localized bleeding resulting from inserting microscale neural probes into the cortex and to explore an approach to minimize blood vessel disruption through insertion methods and probe design. We used *in vivo* two-photon microscopy in the mouse cortex to characterize neurovascular architecture to a depth of 500 μm from the cortical surface. We examined neurovasculature maps prior to probe insertion and then used these vascular maps to select preferred insertion positions and trajectories to reduce localized neurovasculature damage. We show that the details of insertion location and trajectory do affect initial neurovascular damage. Additionally, we found that large penetrating vessels do not penetrate into the cortex exactly perpendicularly from the surface, but deviate slightly from the normal axis in a statistically predictable manner. This results in the possibility of probes disrupting major neurovasculature below the cortical surface upon insertion even when they are positioned to avoid surface blood vessels. These results are important for providing experimental data for the rational design of improved probes and surgical techniques to minimize localized bleeding, and as such, increase the likelihood of improved long-term function.

2. Materials and methods

2.1. Surgery

All animal techniques were developed and practiced in accordance with the policies of the University Committee

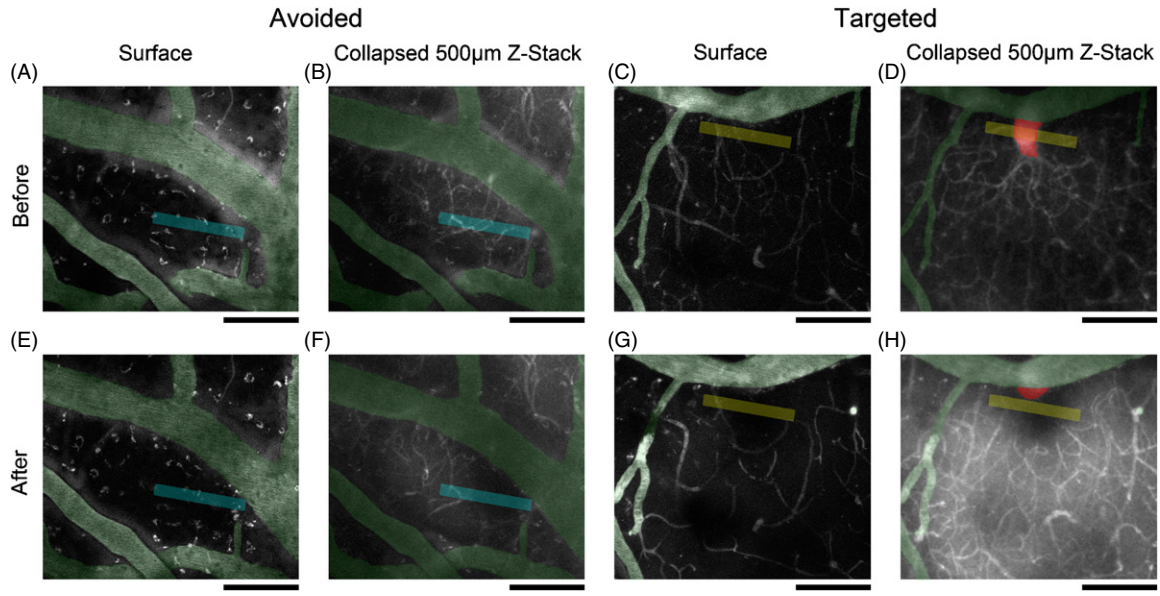

Figure 1. Two-photon imaging of cortical vasculature in a single mouse before probe insertion (A)–(D) and after probe insertion, 30 min incubation and probe explantation (E)–(H). Capillaries (<5 μm diameter) are indicated as white. Major vessels (>5 μm diameter) are highlighted; surface vessels (green) and vessels below the pia (red). (A), (C), (E), (G) Image of the surface vasculature. (B), (D), (F), (H) Collapsed image of neurovasculature 0–500 μm for (A), (C), (E), (G), respectively. Blue indicates probe insertion sites for avoiding major vessels and only disrupting capillaries. Yellow indicates probe insertion sites for disrupting a major blood vessel not visible from the surface. Red blood cells can be visualized by dark regions in collapsed images. Scale bar indicates 100 μm.

on Animal Resources at the University of Rochester. Five adult male CD1 mice 38–44 g (Jackson Labs, Bar Harbor, ME) were anesthetized intraperitoneally with 90 mg ketamine hydrochloride and 9 mg xylazine (Hospira, Lake Forest, IL) per kg body weight.

After removal of the skin and connective tissue on the surface of the skull, the skull was glued to a metal plate that was then fastened into a metal base that connected directly into the microscope stage for imaging. The skull was thinned using a high-speed dental drill (Fine Science Tools, Foster City, CA) and removed with forceps to create a 2 mm by 3 mm craniotomy between lambda and bregma lateral to midline. The skull was periodically bathed in saline to ensure that the underlying cortex did not experience thermal damage from drilling. Because mouse dura (few cell layers thick, $\ll$80 μm) is substantially thinner than rat dura ($\sim$80 μm), it was left intact to prevent the brain from expanding due to excessive hydration (Maikos *et al* 2008). During imaging, anesthesia was maintained with periodic injections of ketamine/xylazine. Occasionally, removing the skull cap resulted in bleeding from the dura or cortex. Once bleeding subsided, the mice were injected with 0.5 mL of 5 mg mL^{-1} FITC-albumin retro-orbitally.

2.2. *Two-photon neurovascular mapping and insertion*

A custom two-photon laser scanning microscope (Majewska *et al* 2000b) was used for *in vivo* imaging. The microscope consisted of a modified Fluoview confocal scan head (Olympus Optical) and a Ti:S laser providing 100 fs pulses at 80 MHz at a wavelength of 920 nm (Mai Tai; Spectra-Physics, Menlo Park, CA). Fluorescence was detected using non-descanned photomultiplier tubes (HC125-02; Hamamatsu, Shizouka, Japan) in whole-field detection mode. The craniotomy over the exposed cortex was initially identified under a dissection scope, and a detailed neurovasculature map was created using a 20×, 0.95 numerical aperture lens (IR2; Olympus Optical). Images were acquired using the Olympus Fluoview software. *Z* stacks taken 5 μm apart from the pia to a depth of 500 μm below the surface were acquired immediately before and immediately after electrode explantation. A 3D neurovascular map was reconstructed from the image stack and two probe insertion regions were selected for each animal: (1) a region containing a large diving blood vessel not visible from the surface and (2) a region devoid of any major blood vessels containing minimal blood capillaries (figures 1 and 2). These regions were $\sim$200–1000 μm apart and were co-registered using major surface vessel landmarks. Two different single tapered penetrating shank 15 μm thick, 3 mm long Michigan-style micromachined silicon probes with a base width of 123 μm (A1 × 16 3mm100–177, NeuroNexus Technologies, Inc., Ann Arbor MI), provided by the University of Michigan, Center for Neural Communication Technology (CNCT), were inserted into these regions using a stereotaxic micropositioner at a manual speed of $\sim$1–1.5 mm s^{-1} (hand-dialed) under visual guidance using an Olympus SZ61 microscope on a $\sim$30° angled tilt mount. Minimal dimpling was observed. Because the center-to-center spacing of the electrodes sites is known to be 100 μm, the depth of insertion was confirmed by counting the number of exposed electrode sites on the probe using the tilted surgical microscope. In each trial, the order of electrode implantation was randomized. The second device insertion was completed within 45 s of the first device being implanted. Probes were left in place for 30 min, and then removed in the order they were implanted. Immediately after probe removal, *Z* stacks were again taken 5 μm apart for up to 500 μm below the surface (figures 1 and 2). If excessive surface bleeding was

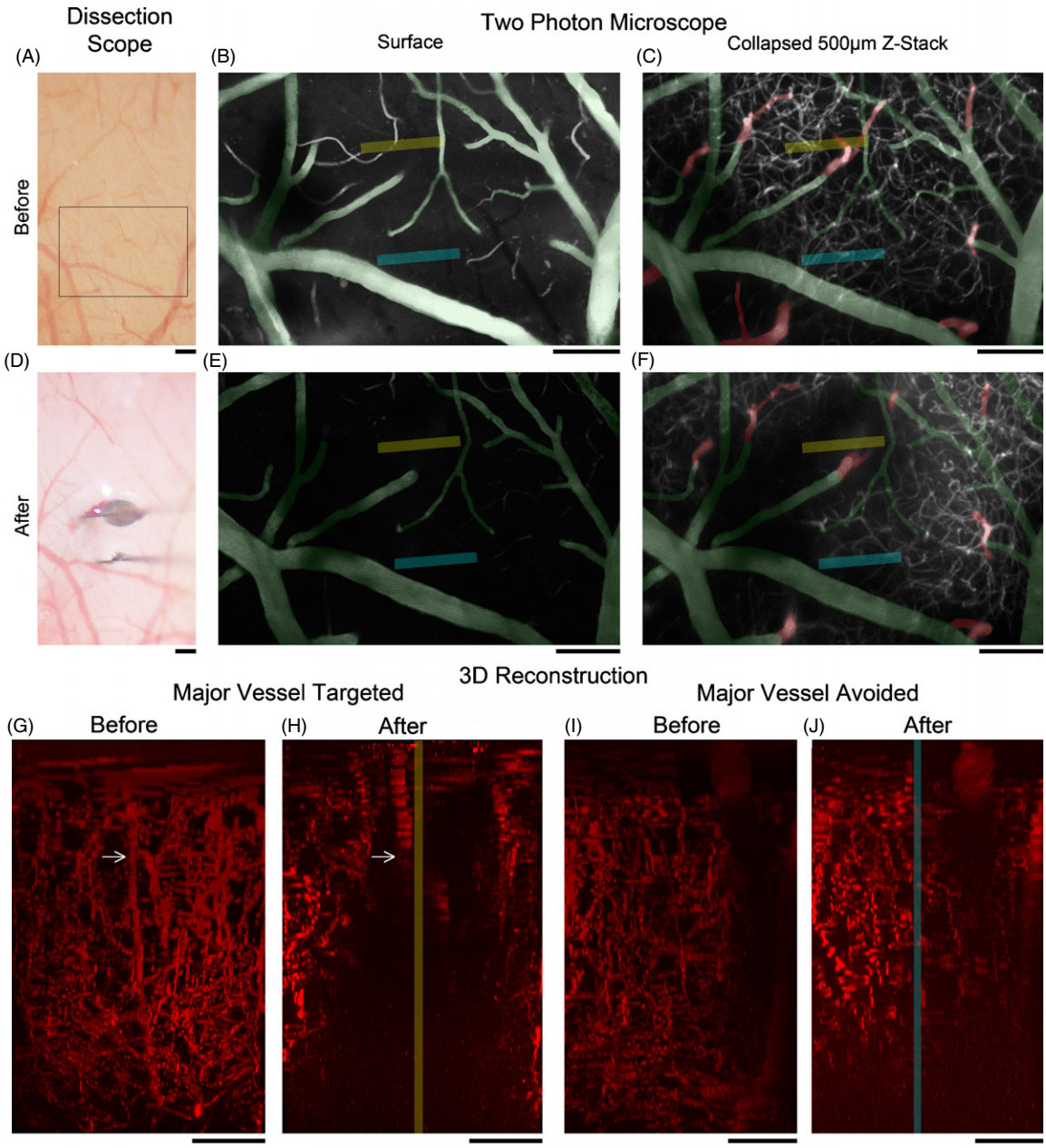

Figure 2. Imaging of cortical vasculature in a single mouse before probe insertion (A)–(C), (G), (I) and after insertion (D), 30 min incubation and probe explantation (E), (F), (H), (J). Blue indicates probe insertion sites for avoiding major vessels and only disrupting capillaries. Yellow indicates probe insertion sites for disrupting a major blood vessel not visible from the surface. (B), (C), (E), (F) Capillaries (<5 μm diameter) are indicated as white. Major vessels (>5 μm diameter) are highlighted: surface vessels (green) and vessels below the pia (red). (A), (B), (D), (E) Image of the surface vasculature. (C), (F) Collapsed image of neurovasculature 0–500 μm for (B), (E), respectively. (G)–(J) 3D reconstruction of vasculature in IMARIS (Bitplane, Saint Paul, MN) to a depth into the image of 180 μm surrounding the probe. Dark regions devoid of capillaries indicate bleeding or loss of perfusion from neurovascular damage. Scale bars indicate 100 μm. Note the loss of signal was greater when major vasculature was targeted (H) compared to when the vasculature was avoided (J). White arrows indicate the targeted major vessel.

observed following imaging, the coagulated blood was gently swabbed off and the brain surface was imaged again. This was possible without causing additional bleeding because the dura was left intact.

2.3. Data analysis

In each animal, prior to insertion, the depth at which the projected probe track would sever the major vessel was noted through examination of the image stacks. This depth was then also used for the control insertion comparison in which the electrode did not target a major vessel. Following the experiments, the image slice at the noted depth prior to the probe insertion and after probe removal was then compared side by side for both the targeted and avoided insertions (figures 3(A) and (B)). TPM can only image the shadows where blood cells suppressed the fluorescent signal; therefore, the

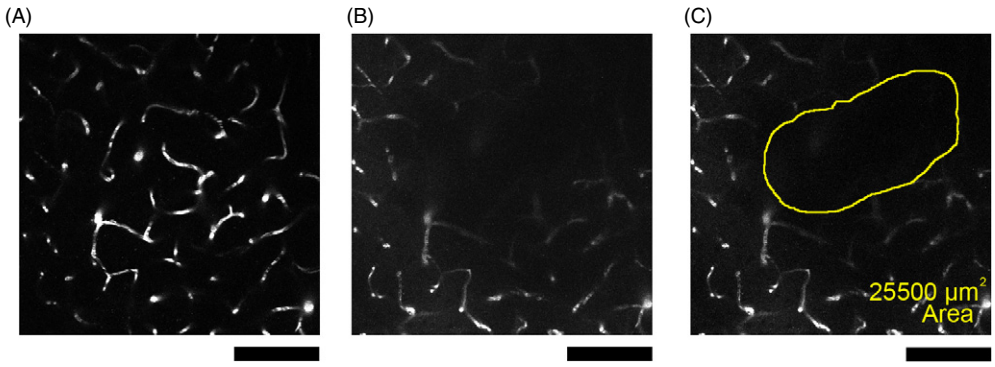

Figure 3. Two-photon imaging of cortical vasculature at a depth in which the targeted probe would have disrupted the major vessel in a mouse before probe insertion (A) and after probe insertion, 30 min incubation and probe explantation (B). Neurovascular damage was visualized by dark regions, where previously blood vessels could be seen. (C) Same image as (B), but dark regions where blood cells suppress fluorescent signals have been circled by a blind observer. Scale bars indicate 100 μm.

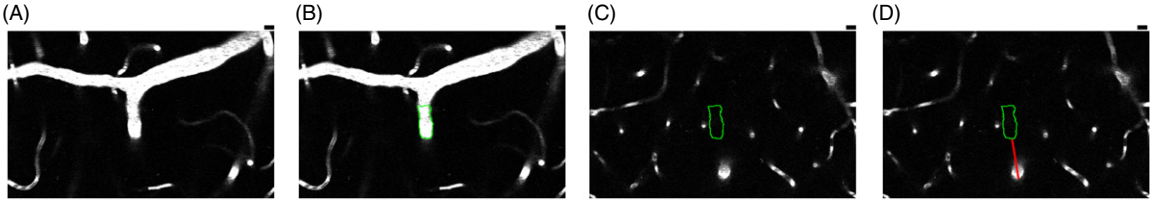

Figure 4. Measuring the 'deviation radius' of major neurovasculature using TPM. (A) Neurovasculature on the surface of the brain. (B) Relevant major surface vessels were traced, and (C) traces projected onto subsequent deeper image slices (250 μm). (D) Deviation radius was measured as the maximum distance between the penetrating vessel wall and the nearest surface vessel wall. Scale bars indicate 10 μm.

area of neurovascular damage was measured through marking the depth in which the projected probe track would have severed the major vessel, instead of calculating the volume of the damage. The area of neurovascular damage was measured and calculated in ImageJ (NIH) using the *'Measure'* functions by a blind observer by circling dark regions using the *'Freehand Selection'* tool where blood cells either due to bleeding or loss of perfusion suppressed fluorescent signals from capillaries that were visible prior to insertion (figure 3) (Kleinfeld *et al* 1998). This area in each animal was then compared between when major vessels were avoided and when major vessels were targeted (figure 5). Percentages were calculated by 'damage area for major vessel avoided insertion'/'damage area for major vessel targeted insertion' for each animal at the same depth. In all cases, the damaged areas between the two probe insertion sites at the noted depth did not overlap. We also measured bleeding at the surface of the brain after electrode explantation using a similar blind scoring method on the most dorsal image slice in the stack (figure 5). A paired two-tailed *t*-test comparison was used to determine statistical significance at $p < 0.05$. Data are presented as mean $\pm$ standard deviation.

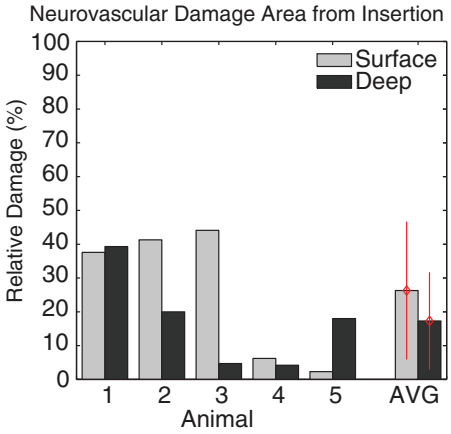

Figure 5. Relative size of neurovascular damage measured using *in vivo* two-photon imaging from when probe insertion disrupted only capillaries normalized to when insertion targeted a major blood vessel in the same animal 30 min after insertion. Light: hemorrhaging at the surface was reduced on average 73% ($p = 0.22$) when avoiding major vessels. Dark: neurovascular damage at the vessel disruption depth, 80–255 μm below the tissue surface, was reduced on average 82.8% ($p = 0.049$). Red bars indicate standard deviation.

2.4. Neurovasculature characterization

In an effort to estimate the necessary insertion distance from surface vessels to statistically decrease the chance of disrupting major penetrating vessels during probe insertion, the penetrating neurovasculature was studied through two-photon imaging. Blood vessels were identified from collected images under digital zoom (600%) using ImageJ. Surface vessels were first noted in superficial slices and traced onto subsequent deeper image slices. To determine average vessel deviation from normal relative to the surface, vessels up to 400–500 μm below the surface were studied. Vessels with a diameter of less than 5 μm were considered capillaries

(Chaigneau *et al* 2003). If the surface of the brain was slightly tilted during imaging, the measurements were geometrically adjusted as needed. Tilt angles were calculated using the Pythagorean theorem by noting the depth at which the surface of the brain came into focus in each corner of the image, and the width and the height of each image. In this experimental setup, the view angle alignment has an error up to 0.22°.

Major surface vessels extend into the brain tissue, usually at an angle from the vector normal (defined as the z-axis) to the brain surface (defined as the x–y plane). To quantify the position of these vessels in the x–y plane, the 'deviation radius' was defined as the distance from the edge of a major surface vessel in the x–y plane that each major penetrating vessel occupied (figure 4). This was measured as the maximum distance between the penetrating vessel wall and the nearest surface vessel wall which was traced in the complete xyz image stack. For each selected vessel in each image slice, the deviation radius and vessel diameter were recorded.

3. Results

3.1. Probe insertion targeting or avoiding neurovasculature

Probe insertion location was examined using TPM to determine the effects of targeting or avoiding major penetrating vessels on neurovascular damage. Hemorrhaging at the surface of the brain was highly variable. The time course of bleeding could not be examined due to blood cells' intrinsic property to suppress two-photon-induced fluorescent signals. Images were used to quantify the area of loss of fluorescent signal from neurovascular damage caused by probe insertion. The results indicate that neurovascular damage and bleeding can be reduced by inserting the probe to avoid major penetrating blood vessels that are not visible on the surface. On average ($N = 5$), the neurovascular damage area was reduced by 82.8 ± 14.3% ($p = 0.049$) in deep cortical areas when avoiding major vessels compared to targeting major vessels. This corresponds to a neurovascular damage area that is about 17% that of the damage area when a major vessel was targeted. At the surface of the brain, the neurovascular damage area was reduced by 73.7 ± 20.3% ($p = 0.22$) when major vessels were avoided relative to when vessels were targeted. This corresponds to a damage area that is about 26% of the area when a major vessel is targeted (figure 5).

3.2. Neurovascular characterization

3.2.1. Blood vessel deviation. The 'deviation radius' was defined as the distance of the penetrating vessel at a given depth from the edge of a major surface vessel (defined as >5 μm) in the x–y plane and measured as the distance between the furthest penetrating vessel wall and the nearest surface vessel wall traced throughout the complete xyz image stack. The deviation radius as a function of depth for each major vessel was plotted together relative to their respective surface origin (figure 6(A)). Surface neurovasculature tended to lie horizontally along the surface plane (figures 1 and 2). However, major vessels just below the surface of the brain tended to be vertically aligned with limited horizontal displacement. The average slope of the deviation radius was 0.102 μm μm^{-1} with respect to depth. Major blood vessels were binned according to their maximum horizontal displacement from the vertical plane perpendicular to the surface or vessel deviation radius (figure 6(B)). The average maximum deviation radius from a vessel's surface origin was 39.3 ± 24.3 μm at 500 μm depth.

3.2.2. Blood vessel diameter. The maximum deviation radius was also compared to the respective surface vessel diameter to determine if the diameter of the originating surface vessel influences the maximal deviation radius (figure 6(C)). An $R^2 < 0.001$ showed a lack of correlation between the deviation distance and the vessel diameter. The major vessel diameter was also compared as a function of depth to determine if the diameter of penetrating blood vessels decreases greatly with depth (figures 7(A) and (B)). If so, disrupting a major vessel deeper in the cortex may result in less neurovascular damage. However, while a general trend can be observed where the vessel diameter decreases as a function of depth (0.0149 μm lateral per micron depth, $R^2 = 0.454$), the diameter only decreases 15 nm per μm depth. Additionally, neurovascular models can be developed from these observations to optimize neural probe insertion targets with respect to minimizing BBB disruption.

4. Discussion

4.1. Two-photon neurovascular mapping and insertion

All types of implantable neural probes for recording exhibit variability and limited reliability with respect to long-term recording performance and tissue responses. In this study, we examined one possible component of this variability: immediate neurovascular damage from bleeding or loss of perfusion as a function of probe insertion relative to surface and penetrating blood vessels. Inasmuch as capillary disruption causes less local neurovascular damage in the region around the probe than severing a major blood vessel, we used two-photon imaging to investigate approaches to minimize vessel damage through precisely positioning and inserting the probe relative to large blood vessels. Specifically, we found that by using a tilted stereo microscope and micro-manipulator, it is possible to bias probe insertions to avoid (or alternatively, to target) penetrating major vessels. While this study was not intended to directly link chronic recording performance to initial neurovascular damage, it is the first study to demonstrate that it is possible to vary the degree of local neurovascular damage by strategically selecting the probe insertion location. Moreover, this study suggests that *not* controlling the insertion location of each penetrating probe shank is very likely to result in a range of neurovascular damage around the individual shanks. It provides a solid step forward toward understanding the relationships between probe design, neurovascular damage and functional performance.

At a depth where the probe disrupted major penetrating vessels, the average damage area observed was 57 000 μm^2, compared to an average damage area of 9300 μm^2 at the same depth when major penetrating vessels were avoided.

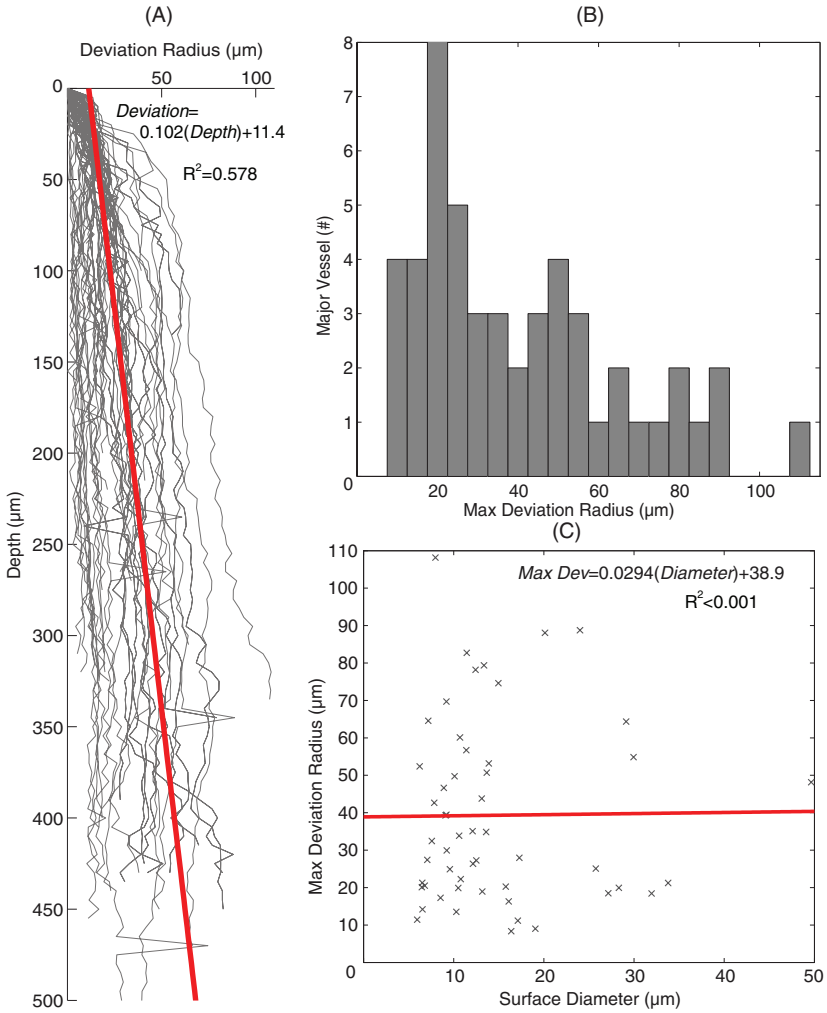

Figure 6. Neurovascular characterization. (A) Traces of vessel deviation from its surface origin as a function of depth. Red trend line represents the average slope. (B) Histogram plot of major blood vessels' maximal deviation from their surface origin. (C) Surface vessel diameter is examined against maximum deviation radius from its surface origin. The correlation coefficients were calculated by ordinary least-squares linear regression. Trend line shows poor correlation between surface vessel diameter and deviation.

Interestingly, hemorrhaging on the surface is not indicative of overall bleeding within the extent of the cortex as it appeared to be highly variable and did not show statistically significant changes between the two implantation sites ($p = 0.22$). This may be due to multiple causes, including the hydration level as well as the size and depth of the major vessel that was disrupted. Thus, surface bleeding does not appear to be a reliable indication of cortical damage sustained during electrode implantation.

4.2. Neurovasculature characterization

This is the first time the neurovascular pattern has been characterized in the cortex for the purpose of neural probe insertion. Previous studies in many mammals, including mice and humans, found that large intracortical vessels penetrate perpendicularly from the cortical surface and extend deep into cortical layers and even into white matter (Helmchen and Kleinfeld 2008, Duvernoy *et al* 1981, Bolan *et al* 2006, Dorr *et al* 2007, Nishimura *et al* 2007). For this reason, the standard practice for probe and microelectrode insertion is to only avoid severing surface vessels during insertion. However, this study shows that large subsurface cortical vessels do not penetrate into the cortex exactly perpendicularly, but deviate slightly from the normal axis. Therefore, probe insertions can disrupt major neurovasculature below the surface of the cortex even when the surface vessels are not penetrated. We found that non-capillary blood vessels tended to deviate at an average of 7.0° from normal relative to the cortical surface. Sixty-eight percent of the major blood vessels remained within 49 μm of the normal axis to the surface for the first ~500 μm in depth, and 95% of the vessels remained within 97 μm of normal. This experimental setup had an angle alignment error of 0.2°, which is small relative to the practical limitations of manually aligning probes to be perpendicular to the surface of the brain with a micropositoner. Neurovascular deviation was also not found to be related to the vessel diameter, but the vessel diameter generally does appear to gradually decrease as a function of depth.

Going beyond the use of two-photon microscopy, these findings suggest a set of neurosurgery guidelines to improve probe insertion outcomes by reducing local neurovascular

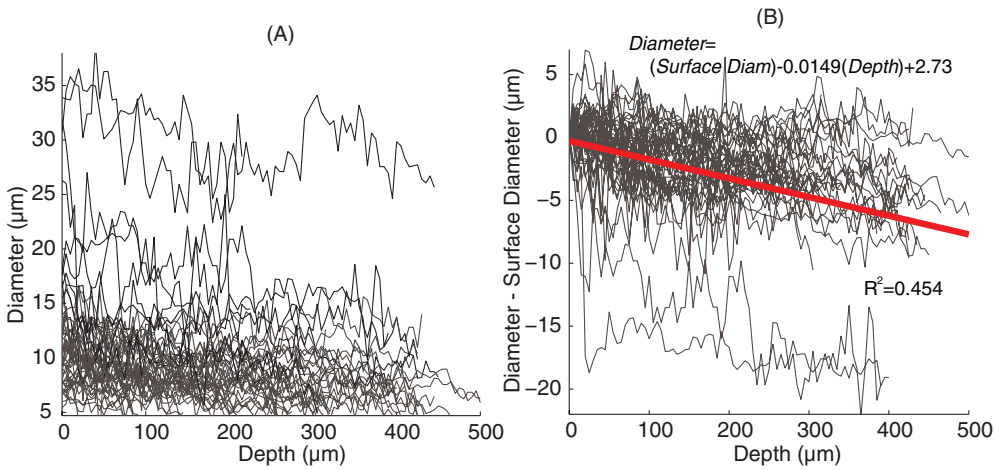

Figure 7. Neurovascular characterization of non-capillary vessel diameters (>5 μm diameter). (A) Traces are colored according to their starting diameter: 5–15 μm (gray) and >15 μm (black). (B) The diameter of the blood vessels is plotted after subtracting their surface diameter, showing a general decreasing trend of vessel diameter as a function of depth. The correlation coefficients were calculated by ordinary least-squares linear regression.

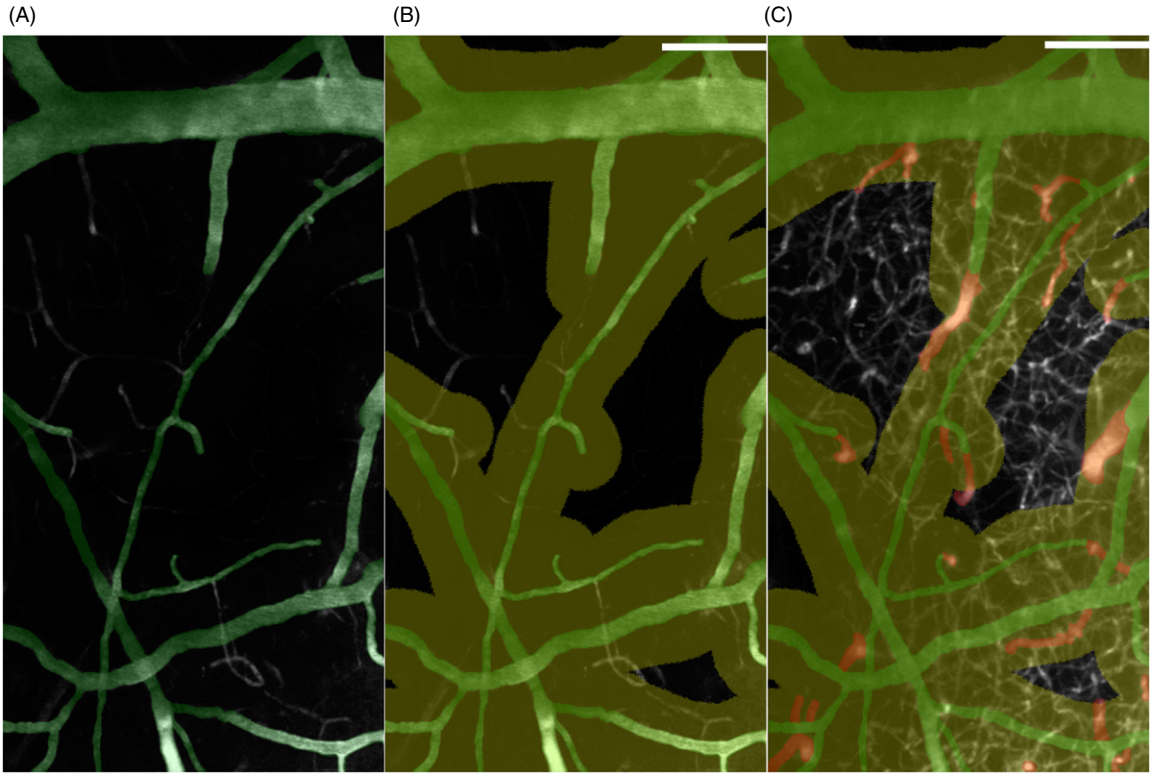

Figure 8. Two-photon image of the vasculature of the mouse cortex. Major vessels (>5 μm diameter) are highlighted: surface vessels (green) and diving vessels (red). Capillaries (<5 μm diameter) are represented in white. (A) Surface image of the mouse cortex. (B) Surface image with a 49 μm 'no implant' region highlighted in yellow. Outline indicates range of 68% confidence interval for vessel deviation. (C) Collapsed image of labeled vessels to a depth of 500 μm shown with the same outline.

damage. Since 68% of the major (non-capillary) vessels remain within a 48.6 μm radius from their surface origin along the normal axis, avoiding insertion within about 49 μm from any surface vessel will significantly decrease the chance of disrupting the penetrating segment of the vessel during insertion. To demonstrate this approach, an additional cortical TPM image was obtained in one case (figure 8). A region was highlighted spanning 49 μm from each vessel wall to mark a 'no implant' zone. A collapsed 500 μm image of outlined blood vessels demonstrates the effectiveness of this technique to reduce the probability of disrupting a major blood vessel during insertion, showing that major blood vessels are not targeted within this zone even deep inside the brain.

Using currently available multiphoton microscopes, combined with the limited concentrations of fluorescent dyes that can be achieved within the vasculature, the depth of

penetration for imaging subsurface vessels was limited to about 500 μm. For this reason, a mouse model was used in this study over rats or higher mammals because the cortex is proportionally thinner in mice. For example, in the mouse cortex, cell bodies of layer V neurons are located only 700–800 μm below the surface of the cortex (Levene *et al* 2004). This results in more complete imaging of the entire neurovasculature within the mouse cortex, whereas in larger mammals, deeper output layers of the cortex would be unlikely to fall within the potential imaging depth. The 'no implant' zones we report for the mouse may have to be updated and scaled appropriately for optimal electrode insertion and electrode design in humans. Penetrating cortical vessels in humans typically have a diameter of 40 μm or less in diameter which is similar to measurements in cats and dogs (Duvernoy *et al* 1981) and is similar to the mouse penetrating cortical vessels observed in this study. However, the depth of the human cortex ($\sim$2 mm) (Lauwers *et al* 2008) is different from the depth of the mouse cortex (900 μm) (Zhang and Sejnowski 2000), which may affect the 49 μm 'no implant zone' we reported here on the mouse model. Additionally, the size of the animal may also influence the degree to which the brain moves due to blood pulsation and breathing affects this 'no implant zone'. To date, mouse cerebral vasculature studies have focused on the circle of Willis, and detailed studies examining mouse cortical vasculature are still necessary in order to compare it to human cortical vasculature (Dorr *et al* 2007).

4.3. Future directions

4.3.1. Complete cortical neurovascular mapping and histology. Even though this study only examined a 500 μm depth from the cortical surface, new studies are underway using similar dye injection techniques combined with advanced postmortem histological techniques, to map and characterize the entire neurovasculature in the brain (Tsai *et al* 2009). Findings from these studies may indicate whether examining the first 500 μm would provide enough information to substantially reduce the risk of damage for deeper insertions. Additionally, further histology is necessary to piece together accurate shape and volume of bleeding in the cortex since TPM can only image the optical shadows where blood cells suppressed the fluorescent signal. Histological analysis would also provide a more accurate and complete understanding, as well as determine the accuracy of TPM imaging when there is blood on or near the surface of the brain. Furthermore, blood plasma and its components, such as blood cells and FITC albumin, can be smeared during probe insertion or can diffuse away from the rupture site. Because their antagonistic effects on the CNS tissue are well documented in the literature as described in the introduction, future studies should focus on the presence and location of non-perfusing blood cells and plasma molecules in the assessment of neurovascular damage in the cortex. It is possible that the blood vessels are disrupted from tearing during electrode insertion as well as rupturing from compression. Further investigation *in vivo* will be necessary to determine their exact contribution. Finally, histologic evaluations of the brain tissue surrounding the probes implanted chronically for various durations will provide a more accurate depiction of bleeding damage by limiting secondary damage caused by explantation. This will also enable combining chronic electrophysiological recording to histological analysis.

4.3.2. Blood brain barrier disruption and long-term neural implants. In this study, we have validated that TPM can be used to map the neurovasculature in a live animal preparation in order to determine preferred locations for inserting neural probes to limit vascular damage. We have also shown that it is possible to systematically target and avoid subsurface vasculature in order to control the degree of neurovascular damage from device implantation. The ability to specifically target large subsurface blood vessels, while not desirable for creating a chronic, reliable interface, enables the ability to control the experimental test space and will allow researchers to better design future experiments to understand the effects of BBB disruption and the related blood products on the electrode–tissue interface.

While this study does not directly link neurovascular damage to electrode function, it does enable and motivate subsequent experiments to determine if reducing acute vascular disruption can reduce variability in long-term recording capabilities and tissue reaction. Even among the same microelectrode array, recording sites can fail as early as several weeks or last as long as a few years. Further understanding of this variability in long-term recording capabilities may improve the efficacy of implanted neural microelectrode sites and provide insight into the molecular level for developing strategies to further prolong long-term recording capabilities. Increased tissue trauma and vascular disruption most likely create a larger degree of encapsulation of the implanted device. This sheath around the electrode site could result in an increase in the impedance of the site with consequent increases in thermal noise and decreases in the signal due to shunt loss pathways. Additionally, vascular disruption can also cause neuronal loss though ischemia to tissue downstream of the disrupted vessel, causing extended neural loss around other recording sites that may have avoided major vascular disruption (Nishimura *et al* 2007). By minimizing trauma that occurs during electrode implantation, we expect that these negative effects can be minimized and the consequential variability reduced, resulting in a more stable and efficacious electrode–tissue interface to improve the number of effective recording sites and increase the average recording site lifetime of chronically implanted electrode arrays.

Furthermore, by using advanced TPM techniques, it is possible to study how neurovascular damage affects encapsulation and how encapsulation grows around an electrode track. Chronic TPM studies may reveal where encapsulation originates: at the probe tip, the probe base (pia), at the largest severed blood vessel, near all severed blood vessels and/or from nearby large uncut leaking blood vessels suffering from chronic violation, such as micromotion. It may also reveal the time course for encapsulation and answer how

long encapsulation takes to grow around the entirety of the electrode shaft. Findings from these continuation studies can help investigators focus and test their intervention strategies to further improve chronic recordings.

4.3.3. Implications on neural probe designs. This study also has broad implications for probe design. If we assume an association between vascular disruption and long-term recording capabilities, these results imply that anti-biofouling coatings will be an important part of chronic implantable microelectrodes. Additionally, chronic microelectrodes should be designed to have a small footprint and perhaps be made of a flexible substrate suitable for navigating between or around major penetrating blood vessels. Alternatively, chronic probes designed to have small flexible shanks and tips designed to deflect off diving vessels may allow probes to bend to follow a vessel into the cortex rather than penetrate the vessel. This study suggests that the use of multi-shank electrodes could increase the random chance of having at least some shanks implanted outside 'no implant' zones. However, it also increases the odds that some shanks will not be well positioned. If any shank disrupts a major arteriole during probe insertion, it can cause additional broad range neuronal damage, by means of ischemia, through loss of perfusion to tissue downstream of the disrupted vessel, causing extended neural loss (Nishimura *et al* 2007) and affecting other recording sites. On the other hand, single shank multi-site microelectrodes allow easier navigation of neurovasculature, but it limits the horizontal region in which one can record from the cortex. An alternative design may be a multi-shank microelectrode in which each shank can be individually positioned. Additionally, it may be possible to develop insertion assist devices that perfectly align stereotaxic frames for perpendicular insertions into the surface of the brain by finely controlling the x and y rotational axes. Alternatively, it may be possible to generate and align, perhaps automatically or by generating input coordinates, stereotaxic micropositioners for an optimal angled insertion that will run parallel to a penetrating major vessel. The tradeoff is complexity and surgical time unless an automated system can be developed.

If vascular disruption turns out to not be correlated with long-term recording capabilities, it would allow investigators to focus on other aspects of chronic probe design such as growth factor coatings (Azemi *et al* 2008), stem cell seeding (Purcell *et al* 2009), drug delivery (Rohatgi *et al* 2009), advanced probe architectures (Seymour and Kipke 2007) and flexibility (Kozai and Kipke 2009, Subbaroyan *et al* 2005, Lee *et al* 2005). The final probe design that addresses the chronic interface problem is likely to be a fine-tuned combination of these many parameters. However, further investigation of vascular disruption to long-term recording capabilities will allow investigators to prioritize or eliminate these parameters in future probe designs.

5. Conclusion

This study explores the cortical neurovasculature in order to allow for the ability to decrease localized vascular damage from probe insertions. While neurovascular damage can be easily increased by administering drugs like heparin, using a larger device, or applying horizontal movement during and after probe insertion, this approach to electrode insertion does the opposite and provides a method to reduce bleeding, ischemia and BBB leakage. Avoiding neurovasculature may have additional benefits for neural implants since neuronal nuclei statistically lie further away from vessels than would be expected from a random spatial distribution (Tsai *et al* 2009). Therefore, if we avoid subsurface neurovasculature near electrode recording sites, there is an increased likelihood of being closer to neuronal nuclei. However, a better understanding of patterns of vascular deviation as vessels leave the surface to extend into the parenchyma will allow neurosurgeons not only to optimize their implant locations for cortical prostheses in order to obtain better long-term efficacy, but potentially help to minimize adverse side effects due to cortical vascular disruption and bleeding resulting from trauma of deep brain electrode implantation.

Acknowledgments

The authors would like to thank Badri Roysam for helpful project discussions, Anna Devor for helpful two-photon vascular imaging discussions and Paras Patel for assistance characterizing neurovasculature. This research is supported by Center for Neural Communication Technology, a P41 Resource Center funded by the National Institute of Biomedical Imaging and Bioengineering (NIBIB, P41 EB002030) and supported by the National Institutes of Health (NEI; EY019277), Burroughs Wellcome Fund Career Award in the Biomedical sciences, Fellowship from the Alfred P Sloan Foundation, the Whitehall Foundation, Department of Defense Era of Hope Scholar Award and Pew Scholar in the Biomedical Sciences Award.

Conflicts of interest

DRK has a significant financial and leadership interest in NeuroNexus Technologies, a company specializing in neural interface devices. At the time of this study, NBL was a consultant to NeuroNexus Technologies and TCM was an employee of NeuroNexus Technologies.

References

Abdul-Karim M A, Al-Kofahi K, Brown E B, Jain R K and Roysam B 2003 Automated tracing and change analysis of angiogenic vasculature from *in vivo* multiphoton confocal image time series *Microvasc. Res.* **66** 113–25

Azemi E, Stauffer W R, Gostock M S, Lagenaur C F and Cui X T 2008 Surface immobilization of neural adhesion molecule L1 for improving the biocompatibility of chronic neural probes: *in vitro* characterization *Acta Biomater.* **4** 1208–17

Barzo P, Marmarou A, Fatouros P, Hayasaki K and Corwin F 1997 Contribution of vasogenic and cellular edema to traumatic brain swelling measured by diffusion-weighted imaging *J. Neurosurg.* **87** 900–7

Betz A L, Iannotti F and Hoff J T 1989 Brain edema: a classification based on blood-brain barrier integrity *Cerebrovasc. Brain Metab. Rev.* **1** 133–54

Biran R, Martin D C and Tresco P A 2005 Neuronal cell loss accompanies the brain tissue response to chronically implanted silicon microelectrode arrays *Exp. Neurol.* **195** 115–26

Bjornsson C S, OH S J, Al-Kofahi Y A, Lim Y J, Smith K L, Turner J N, De S, Roysam B, Shain W and Kim S J 2006 Effects of insertion conditions on tissue strain and vascular damage during neuroprosthetic device insertion *J. Neural Eng.* **3** 196–207

Bolan P J, Yacoub E, Garwood M, Ugurbil K and Harel N 2006 *In vivo* micro-MRI of intracortical neurovasculature *NeuroImage* **32** 62–9

Camp D M and Robinson T E 1992 On the use of multiple probe insertions at the same site for repeated intracerebral microdialysis experiments in the nigrostriatal dopamine system of rats *J. Neurochem.* **58** 1706–15

Chaigneau E, Oheim M, Audinat E and Charpak S 2003 Two-photon imaging of capillary blood flow in olfactory bulb glomeruli *Proc. Natl Acad. Sci. USA* **100** 13081–6

Chauhan V P, Lanning R M, Diop-Frimpong B, Mok W, Brown E B, Padera T P, Boucher Y and Jain R K 2009 Multiscale measurements distinguish cellular and interstitial hindrances to diffusion *in vivo Biophys. J.* **97** 330–6

Dixon C E, Clifton G L, Lighthall J W, Yaghmai A A and Hayes R L 1991 A controlled cortical impact model of traumatic brain injury in the rat *J. Neurosci. Methods* **39** 253–62

Dorr A, Sled J G and Kabani N 2007 Three-dimensional cerebral vasculature of the CBA mouse brain: a magnetic resonance imaging and micro computed tomography study *NeuroImage* **35** 1409–23

Dunn K W and Sutton T A 2008 Functional studies in living animals using multiphoton microscopy *ILAR J.* **49** 66–77

Duvernoy H M, Delon S and Vannson J L 1981 Cortical blood vessels of the human brain *Brain Res. Bull.* **7** 519–79

Edell D J, Toi V V, Mcneil V M and Clark L D 1992 Factors influencing the biocompatibility of insertable silicon microshafts in cerebral cortex *IEEE Trans. Biomed. Eng.* **39** 635–43

Goldsmith J D, Kujawa S G, Mclaren J D and Bledsoe S C Jr 1995 *In vivo* release of neuroactive amino acids from the inferior colliculus of the guinea pig using brain microdialysis *Hear Res.* **83** 80–8

Grill W M, Norman S E and Bellamkonda R V 2009 Implanted neural interfaces: biochallenges and engineered solutions *Annu. Rev. Biomed. Eng.* **11** 1–24

Groothuis D R, Ward S, Schlageter K E, Itskovich A C, Schwerin S C, Allen C V, Dills C and Levy R M 1998 Changes in blood-brain barrier permeability associated with insertion of brain cannulas and microdialysis probes *Brain Res.* **803** 218–30

Helmchen F and Denk W 2005 Deep tissue two-photon microscopy *Nat. Methods* **2** 932–40

Helmchen F and Kleinfeld D 2008 *In vivo* measurements of blood flow and glial cell function with two-photon laser-scanning microscopy *Methods Enzymol.* **444** 231–54

Holson R R, Gazzara R A and Gough B 1998 Declines in stimulated striatal dopamine release over the first 32 h following microdialysis probe insertion: generalization across releasing mechanisms *Brain Res.* **808** 182–9

House P A, MacDonald J D, Tresco P A and Normann R A 2006 Acute microelectrode array implantation into human neocortex: preliminary technique and histological considerations *Neurosurg. Focus* **20** E4

Johnson M D, Kao O E and Kipke D R 2007 Spatiotemporal pH dynamics following insertion of neural microelectrode arrays *J. Neurosci. Methods* **160** 276–87

Johnson M D, Langhals N B and Kipke D R 2006 Neural interface dynamics following insertion of hydrous iridium oxide microelectrode arrays *Conf. Proc. IEEE Eng. Med. Biol. Soc.* **1** 3178–81

Kimelberg H K 1995 Current concepts of brain edema. Review of laboratory investigations *J. Neurosurg.* **83** 1051–9

Kipke D R, Shain W, Buzsaki G, Fetz E, Henderson J M, Hetke J F and Schalk G 2008 Advanced neurotechnologies for chronic neural interfaces: new horizons and clinical opportunities *J. Neurosci.* **28** 11830–8

Klatzo I 1967 Presidental address. Neuropathological aspects of brain edema *J. Neuropathol. Exp. Neurol.* **26** 1–14

Kleinfeld D, Mitra P P, Helmchen F and Denk W 1998 Fluctuations and stimulus-induced changes in blood flow observed in individual capillaries in layers 2 through 4 of rat neocortex *Proc. Natl Acad. Sci. USA* **95** 15741–6

Kozai T D and Kipke D R 2009 Insertion shuttle with carboxyl terminated self-assembled monolayer coatings for implanting flexible polymer neural probes in the brain *J. Neurosci. Methods* **184** 199–205

Lauwers F, Cassot F, Lauwers-Cances V, Puwanarajah P and Duvernoy H 2008 Morphometry of the human cerebral cortex microcirculation: general characteristics and space-related profiles *NeuroImage* **39** 936–48

Lee H, Bellamkonda R V, Sun W and Levenston M E 2005 Biomechanical analysis of silicon microelectrode-induced strain in the brain *J. Neural Eng.* **2** 81–9

Levene M J, Dombeck D A, Kasischke K A, Molloy R P and Webb W W 2004 *In vivo* multiphoton microscopy of deep brain tissue *J. Neurophysiol.* **91** 1908–12

Lowery R L, Zhang Y, Kelly E A, Lamantia C E, Harvey B K and Majewska A K 2009 Rapid, long-term labeling of cells in the developing and adult rodent visual cortex using double-stranded adeno-associated viral vectors *Dev. Neurobiol.* **69** 674–88

Maikos J T, Elias R A and Shreiber D I 2008 Mechanical properties of dura mater from the rat brain and spinal cord *J. Neurotrauma* **25** 38–51

Majewska A, Brown E, Ross J and Yuste R 2000a Mechanisms of calcium decay kinetics in hippocampal spines: role of spine calcium pumps and calcium diffusion through the spine neck in biochemical compartmentalization *J. Neurosci.* **20** 1722–34

Majewska A, Yiu G and Yuste R 2000b A custom-made two-photon microscope and deconvolution system *Pflugers Arch.* **441** 398–408

McConnell G C, Rees H D, Levey A I, Gutekunst C A, Gross R E and Bellamkonda R V 2009 Implanted neural electrodes cause chronic, local inflammation that is correlated with local neurodegeneration *J. Neural Eng.* **6** 056003

Mcintosh T K, Smith D H, Meaney D F, Kotapka M J, Gennarelli T A and Graham D I 1996 Neuropathological sequelae of traumatic brain injury: relationship to neurochemical and biomechanical mechanisms *Lab. Invest.* **74** 315–42

Nadal A, Fuentes E, Pastor J and Mcnaughton P A 1995 Plasma albumin is a potent trigger of calcium signals and DNA synthesis in astrocytes *Proc. Natl Acad. Sci. USA* **92** 1426–30

Nadal A, Sul J Y, Valdeolmillos M and Mcnaughton P A 1998 Albumin elicits calcium signals from astrocytes in brain slices from neonatal rat cortex *J. Physiol.* **509** Pt 3 711–6

Narayan R K *et al* 2002 Clinical trials in head injury *J. Neurotrauma* **19** 503–57

Nishimura N, Schaffer C B, Friedman B, Lyden P D and Kleinfeld D 2007 Penetrating arterioles are a bottleneck in the perfusion of neocortex *Proc. Natl Acad. Sci. USA* **104** 365–70

Purcell E K, Seymour J P, Yandamuri S and Kipke D R 2009 *In vivo* evaluation of a neural stem cell-seeded prosthesis *J. Neural Eng.* **6** 026005

Rohatgi P, Langhals N B, Kipke D R and Patil P G 2009 *In vivo* performance of a microelectrode neural probe with integrated drug delivery *Neurosurg. Focus* **27** E8

Schmidt E M, Bak M J and Mcintosh J S 1976 Long-term chronic recording from cortical neurons *Exp. Neurol.* **52** 496–506

Schwartz A B, Cui X T, Weber D J and Moran D W 2006 Brain-controlled interfaces: movement restoration with neural prosthetics *Neuron* **52** 205–20

Seymour J P and Kipke D R 2007 Neural probe design for reduced tissue encapsulation in CNS *Biomaterials* **28** 3594–607

Shen Y, Jacobs J M, Camp D G II, Fang R, Moore R J, Smith R D, Xiao W, Davis R W and Tompkins R G 2004 Ultra-high-efficiency strong cation exchange LC/RPLC/MS/MS for high dynamic range characterization of the human plasma proteome *Anal. Chem.* **76** 1134–44

Subbaroyan J, Martin D C and Kipke D R 2005 A finite-element model of the mechanical effects of implantable microelectrodes in the cerebral cortex *J. Neural Eng.* **2** 103–13

Svoboda K and Yasuda R 2006 Principles of two-photon excitation microscopy and its applications to neuroscience *Neuron* **50** 823–39

Szarowski D H, Andersen M D, Retterer S, Spence A J, Isaacson M, Craighead H G, Turner J N and Shain W 2003 Brain responses to micro-machined silicon devices *Brain Res.* **983** 23–35

Tsai P S, Kaufhold J P, Blinder P, Friedman B, Drew P J, Karten H J, Lyden P D and Kleinfeld D 2009 Correlations of neuronal and microvascular densities in murine cortex revealed by direct counting and colocalization of nuclei and vessels *J. Neurosci.* **29** 14553–70

Turner J N, Shain W, Szarowski D H, Andersen M, Martins S, Isaacson M and Craighead H 1999 Cerebral astrocyte response to micromachined silicon implants *Exp. Neurol.* **156** 33–49

Tyrrell J A, Mahadevan V, Tong R T, Brown E B, Jain R K and Roysam B 2005 A 2-D/3-D model-based method to quantify the complexity of microvasculature imaged by *in vivo* multiphoton microscopy *Microvasc. Res.* **70** 165–78

Unterberg A W, Stover J, Kress B and Kiening K L 2004 Edema and brain trauma *Neuroscience* **129** 1021–9

Zhang K and Sejnowski T J 2000 A universal scaling law between gray matter and white matter of cerebral cortex *Proc. Natl Acad. Sci. USA* **97** 5621–6

Zhang S, Boyd J, Delaney K and Murphy T H 2005 Rapid reversible changes in dendritic spine structure *in vivo* gated by the degree of ischemia *J. Neurosci.* **25** 5333–8

Zipfel W R, Williams R M and Webb W W 2003 Nonlinear magic: multiphoton microscopy in the biosciences *Nat. Biotechnol.* **21** 1369–77